DOI: 10.18462/iir.icr.2023.0696

Operating Strategies of an Industrial R717 Heat Pump Recovering Waste Heat of a Chiller

Manuel VERDNIK*, Philipp WAGNER, René RIEBERER

Institute of Thermal Engineering, Graz University of Technology
Graz, 8010, Austria, manuel.verdnik@tugraz.at

ABSTRACT

Process chains within the food industry, in particular dairies, often demand cooling and heating. While chillers serve the required cooling load, high-temperature heat pumps (HTHPs) can cover parts of the heating demand by lifting the waste heat of chillers to temperature levels suitable for process heat supply.

This study analyses an R717-HTHP, which was directly integrated into the refrigerant circuit of the existing R717 chiller at a dairy. A simulation model in Dymola is used to model the system consisting of the chiller, directly integrated HTHP, thermal energy storage (TES) and the cleaning-in-place (CIP) system as the supplied process. Validation with experimental data qualifies the model for further analysis of the system behaviour.

The simulation model is used to study the influence of the operating parameters (e.g. refrigerant subcooling, medium pressure level, heat sink temperatures and cooling capacity) on the efficiency of the system. Based on these findings, increasing the medium pressure is shown to increase the ability to cover peak loads of the CIP system.

Keywords: Ammonia, Industrial heat pumps, Energy efficiency, Energy savings, Compression systems, Simulation model

1. INTRODUCTION

Waste heat utilization using HTHPs enables the reduction of the energy demand of a facility and can contribute to the decarbonisation of the industry by decreasing fossil-fuelled heat supply. Especially in the food industry often a demand for heating and cooling exists, and waste heat of chillers can be used as the heat source for HTHPs. According to the IEA (2022), heat pumps can in principle cover around 40 % of all processes in the food industry, mainly where temperatures below 150 °C are needed.

Dairies in the EU processed 159 million tons of milk to 119 million tons of products in 2017 (Eurostat, 2018), with the energy demand strongly varying between products. Keller et al. (2016) report an electricity demand between 0.3 MJ/kg for UHT milk (3.5 % fat) and 1.0 MJ/kg for concentrated milk (0.2 % fat), and an additional steam demand of 0.4 MJ/kg for UHT milk and 2.4 MJ/kg for concentrated milk. Besides the actual process steps, cleaning-in-place (CIP) systems used for the equipment also demand heating. Bakalis et al. (2019) report the share of energy demand for milk production to 19 % for cooling, 38 % for homogenisation and pasteurisation and 10 % for CIP processes.

Simulation models can help to gain insights into complex systems. In the present case, the heat pump is directly integrated into the refrigerant cycle of the chiller and the heat pump and the CIP-system are connected with a TES, leading to interrelationships within the system. By means of a dynamic simulation model, these interrelationships can be analysed and insights relevant for optimising the operation can be gathered. Transient simulations allow to investigate the TES especially at varying loads and different operating strategies for the heat pump. What is more, scenarios - which would be time-consuming, risky to test or depend on certain operating parameters of the plant - can be tested independent of the plant operation.

2. SYSTEM DESCRIPTION

Since a couple of years an NH_3 chiller is used to cover parts of the cooling demand of a dairy in Austria. By means of the chiller the water used for process cooling is cooled to a temperature of around 1 °C (see $t_{CH,SO,out}$ in Fig. 1) before it flows into an “ice bank”. Originally the low-temperature waste heat of the chiller could not be used and was rejected to the environment via a cooling tower. In order to reduce the CO_2-emissions of the milk processing, an HTHP was directly integrated into the refrigerant cycle of the existing chiller. The integration of the HTHP allows to lift the low-temperature heat to a temperature level suitable to supply a cleaning-in-place (CIP)-system. This enables a significant reduction of the steam demand for the CIP-system usually covered by gas boilers.

Due to the fact that with available components on the market supply temperatures of up to 95 °C can be achieved with a NH_3 heat pump and an integration in the refrigerant circuit was possible, the HTHP was integrated as an "add-on" system. Compared to a cascade system, this avoids the disadvantage of an additional temperature difference in a cascade heat exchanger. Fig. 1 shows the schematic flow chart including sensor positions of the overall system, which consists of the chiller, HTHP and CIP-system. The state points mentioned in the context of the work always refer to the designations in Fig. 1 (e.g. "CH2"…chiller point no. 2: discharge of low-pressure compressor).

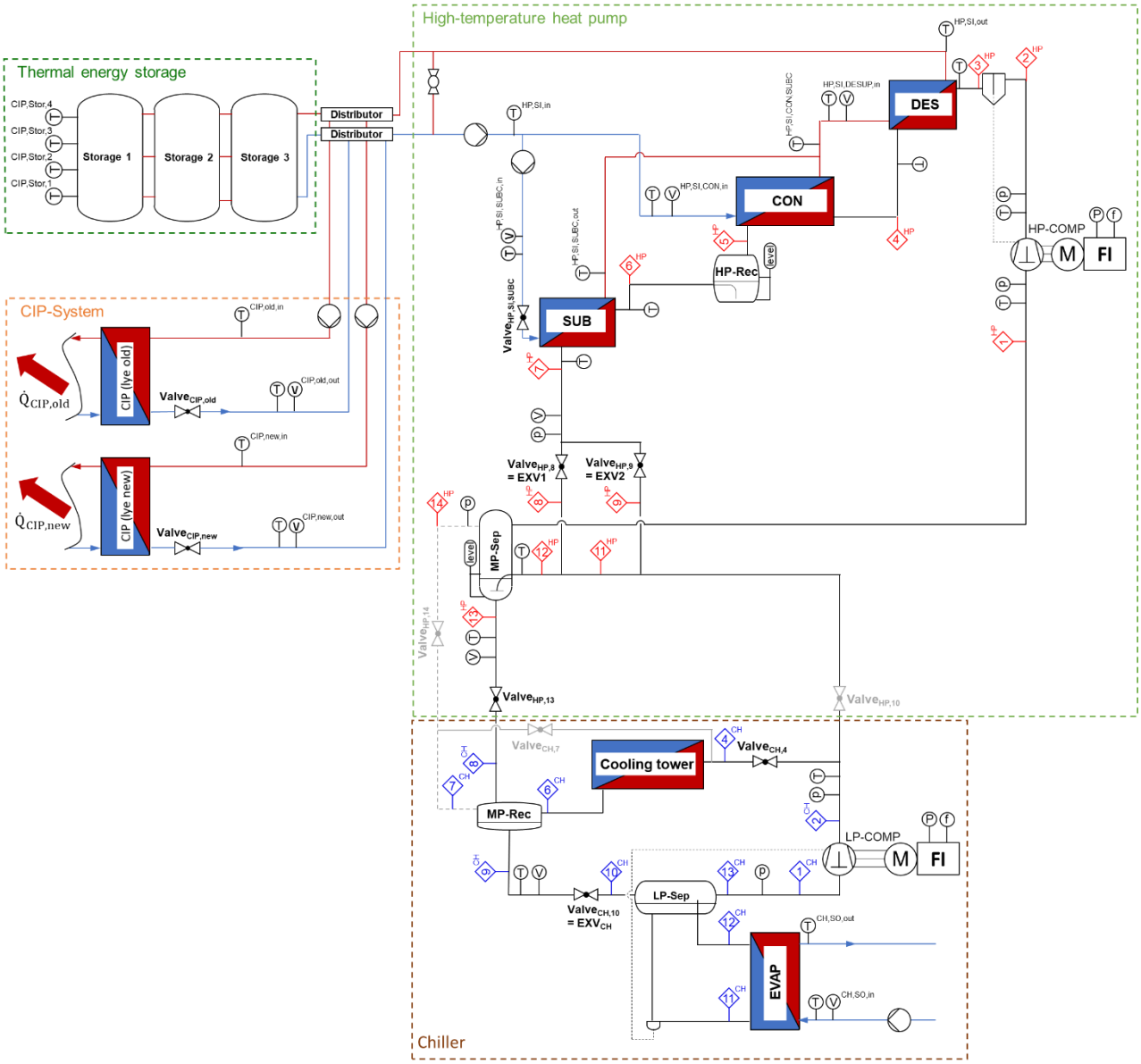

Figure 1: Schematic flow chart including sensor positions of the overall system

The chiller consists of the low-pressure compressor (LP-COMP), a cooling tower (serving as condenser), a medium pressure receiver (MP-Rec), an expansion valve (EXV_{CH}), a low-pressure separator (LP-Sep) and an evaporator (EVAP). The HTHP consists of a medium pressure separator (MP-Sep), a high-pressure compressor (HP-COMP), a desuperheater (DES), condenser (CON) and sub-cooler (SUB), a high-pressure receiver (HP-Rec) and two expansion valves (EXV1 and EXV2). The chiller and the HTHP are connected via the discharge line of the chiller and the medium pressure separator. The distribution of the refrigerant mass flow between the HTHP and the air-cooled condenser (after the low-pressure compressor) is controlled by $Valve_{CH,4}$. By means of $Valve_{CH,4}$ the medium pressure of the system ($p_{CH2} \approx p_{HP1}$) can be adapted. This gives the opportunity to optimise the overall system in terms of efficiency and the capacity provided to the CIP-system. In case there is no demand for process heat, but for process cooling, i.e. the chiller is in operation and the HTHP is switched off, the chiller can be operated independently from the HTHP by closing $Valve_{HP,10}$ and $Valve_{HP,13}$ and opening $Valve_{CH,4}$. Since the chiller is in general always in operation ("24/7"), operation of the HP without the chiller is not foreseen. Both compressors are equipped with a frequency converter to adjust the thermal capacities (heating or cooling) to the actual demand. Furthermore, the subcooling of the refrigerant leaving the sub-cooler can be influenced by means of the water-side volume flow rate through the sub-cooler, which can be adjusted by $Valve_{HP,SI,SUBC}$.

The heat supplied by the HTHP is used to heat the acid and lye tanks of two CIP-systems ("CIP old", "CIP new") and to load the TES consisting of three storage tanks (Storage 1…3). The TES is used to buffer demand peaks and to ensure an easier control for the HTHP. The operation of the HTHP depends on the temperatures in the TES and the requirements of the CIP-systems. Table 1 gives an overview of the design data of the chiller and the HTHP.

Table 1: Design data of the chiller and HTHP

Parameter	Value
Max. cooling capacity chiller ($\dot{Q}_{0,CH}$)	900 kW
Rotation speed low-pressure compressor (chiller, n_{CH})	500…1500 rpm
Max. heating capacity HTHP ($\dot{Q}_{h,HP}$)	550 kW
Rotation speed high-pressure compressor (n_{HP})	550…1800 rpm
Cold water outlet temperature Chiller ($t_{CH,SO,out}$)	1 °C
Heat sink inlet temperature HTHP ($t_{HP,SI,in}$)	60…75 °C
Heat sink outlet temperature HTHP ($t_{HP,SI,out}$)	75…90 °C
Storage tanks volume (overall volume of Storage 1…3)	12 m³

3. SIMULATION MODEL

The simulation model used in this work was set up using the modelica-based TIL-Suite TLK-Thermo (2022a) with components from TLK-Thermo (2022b) for the buffer tanks. The model is based on Verdnik et al. (2022), where steady-state and transient validation with measurement data was presented in detail. A short description of the model and the improvements made are covered in the following section.

The compressors are modelled through their volumetric, overall isentropic and inner isentropic efficiency. The inner isentropic efficiency can be related to the overall isentropic efficiency though a “mechanical” efficiency as depicted in Eq. (4). The polynomial functions used for the low-pressure compressor are given in Eq. (1) to (3) with the pressure ratio of the chiller $\Pi_{\mathrm{CH}} = p_{\mathrm{CH2}}/p_{\mathrm{CH1}}$.

$$\lambda_{vol,CH} = \frac{\dot{m}_{ref,CH}}{\rho_{ref,CH1} \cdot \dot{V}_{swept,CH}} = 6.733 \cdot 10^{-1} - 2.481 \cdot 10^{-2} \cdot \Pi_{CH} \quad \text{Eq. (1)}$$

$$\eta_{is,ov,CH} = \frac{\dot{m}_{ref,CH} \cdot (h_{ref,CH2s} - h_{ref,CH1})}{P_{el,CH}} = 3.173 \cdot 10^{-1} + 1.594 \cdot 10^{-1} \cdot \Pi_{CH} - 1.991 \cdot 10^{-2} \cdot \Pi_{CH}^2 \quad \text{Eq. (2)}$$

$$\eta_{is,i,CH} = \frac{h_{ref,CH2s} - h_{ref,CH1}}{h_{ref,CH2} - h_{ref,CH1}} = 0.81 \quad \text{Eq. (3)}$$

$$\eta_{is,ov,CH} = \frac{h_{ref,CH2s} - h_{ref,CH1}}{h_{ref,CH2} - h_{ref,CH1}} \cdot \frac{\dot{m}_{ref,CH} \cdot (h_{ref,CH2} - h_{ref,CH1})}{P_{el,CH}} = \eta_{is,i} \cdot \eta_m \quad \text{Eq. (4)}$$

The polynomials used for the high-pressure compressor listed in Eq. (4) through (6) consider the pressure ratio $\Pi_{\mathrm{HP}} = p_{\mathrm{HP2}}/p_{\mathrm{HP1}}$ and the compressor speed $\mathrm{n_{HP}}$ [rpm] of the heat pump. For simplification, the oil separator is considered as an isobaric heat-loss and accounted for in the "inner" isentropic efficiency.

$$\lambda_{vol,HP} = \frac{\dot{m}_{ref,HP}}{\rho_{ref,HP1} \cdot \dot{V}_{swept,HP}} = 6.984 \cdot 10^{-1} - 8.247 \cdot 10^{-2} \cdot \Pi_{HP} + 1.701 \cdot 10^{-4} \cdot n_{HP} \quad \text{Eq. (5)}$$

$$\eta_{is,ov,HP} = \frac{\dot{m}_{ref,HP} \cdot (h_{ref,HP3s} - h_{ref,HP1})}{P_{el,HP}} = 0.5383 - 0.03 \cdot \left[\Pi_{HP} - \left(0.5230 + \frac{n_{HP}}{740.1}\right)\right]^2 + \frac{n_{HP}}{18800} \quad \text{Eq. (6)}$$

$$\eta_{is,i,HP} = \frac{h_{ref,HP3s} - h_{ref,HP1}}{h_{ref,HP3} - h_{ref,HP1}} = 0.97 \quad \text{Eq. (7)}$$

The heat exchangers are modelled using the finite volume approach with geometries derived from manufacturer's data. Heat transfer of water and one-phase refrigerant flow is calculated according to Martin (2010). For evaporation and condensation the correlations of Longo et al. (2015) and Akers et al. (1959) are used, respectively. Pressure drop in the heat exchangers is neglected. The cooling tower is modelled trough heat rejection from the medium pressure receiver (MP-rec), allowing to set the pressure level. The outlet of the medium pressure receiver (CH9) is saturated liquid. Throttling processes in the valves are modelled isenthalpic. Regarding the hydraulic layout of the heat sink of the heat pump, $\mathrm{Valve_{SI}}$ (see Fig. 1) is controlled to warm up the heat sink when starting the heat pump. The TES consisting of three buffer tanks with a volume of 4m³ each is modelled as one tank using a model from TLK-Thermo (2022b) with a discretisation of 20 cells, where the heights of sensors and ports correspond to the dimensions of the plant. To consider the heating demand of the CIP system, the heating capacity ($\dot{Q}_{CIP,old}$ and $\dot{Q}_{CIP,new}$) and volumetric flow rate are prescribed.

The COP of the chiller is evaluated according to Eq. (8) using the cooling capacity of the chiller and electric power consumption of the low pressure compressor. The COP of the heat pump is evaluated as shown in Eq. (9) with the heating capacity of the heat pump and the electric power consumption of the high pressure compressor. The COP of the system is evaluated following Eq. (10) with the sum of the cooling and heating capacity and the sum of the electric power consumption of both compressors. Performance factors are evaluated accordingly by integrating the relevant capacity or power to obtain the thermal or electric energy.

$$COP_{c,CH} = \frac{\dot{Q}_{0,CH}}{P_{el,CH}} = \frac{\dot{V}_{CH,SO,in} \cdot \rho_{CH,SO,in} \cdot (h_{CH,SO,in} - h_{CH,SO,out})}{P_{el,CH}} \quad \text{Eq. (8)}$$

$$COP_{h,HP} = \frac{\dot{Q}_{h,HP}}{P_{el,HP}} = \frac{\dot{V}_{HP,SI,in} \cdot \rho_{HP,SI,in} \cdot (h_{HP,SI,out} - h_{HP,SI,in})}{P_{el,HP}} \quad \text{Eq. (9)}$$

$$COP_{sys} = \frac{\dot{Q}_{0,CH} + \dot{Q}_{h,HP}}{P_{el,CH} + P_{el,HP}} \quad \text{Eq. (10)}$$

4. RESULTS OF THE SIMULATION STUDY

This section covers the validation of the simulation model and shows the influence of the controllable refrigerant subcooling ($\Delta T_{sub,HP,7}$ in Fig. 1) with a focus on the hydraulic layout of the heat sink of the heat pump and the influence of the medium pressure level ($p_{CH,2}$ in Fig. 1) at different heat sink temperatures. Finally, the increased ability to cover load peaks of the CIP-system by increasing the medium pressure level and the consequences regarding system efficiency are presented.

4.1. Validation of the simulation model

First, the steady validation of the simulation model presented in Verdnik et al. (2022) is extended to cover more operating points of the chiller. The used operating points are listed in Table 2, Fig. 2 shows a comparison of simulation results with measurement data of the chiller for these operating points.

Table 2: Operating points used for steady-state validation

$t_{CH,SO,in/out}$ in °C	$\dot{V}_{CH,SO,in}$ in m³/h	$t_{HP,SI,in/out}$ in °C	n_{HP} in rpm	$\dot{V}_{HP,SI,DESUP,in}$ in m³/h	$p_{CH,2}$ in bar	$\Delta T_{sub,HP,7}$ in K
4.3/1.0	159.5	62/78	1800	25.9	13.5	13
4.0/1.1	174.3	61/69	900	26.8	13.5	8
4.1/1.1	174.3	68/74	900	26.6	13.5	8
4.0/0.9	172.5	60/80	900	9.2	13.5	16
3.6/1.0	175.9	65/84	1800	25.9	15.5	14
3.0/1.0	174.5	58/84	1800	17.0	13.5	15
2.9/1	167.2	62/90	1800	14.5	13.5	15
4.0/1.1	172.1	71/88	1800	14.9	13.5	13
3.9/1.0	174.3	n.a.	0	n.a.	13.5	n.a.
2.7/1.0	176.1	n.a.	0	n.a.	9.6	n.a.
4.4/1.0	172.6	n.a.	0	n.a.	8.7	n.a.
3.0/1.0	175.3	n.a.	0	n.a.	10.2	n.a.

As can be seen from Fig. 2, the maximum deviation between simulated and measured chiller compressor speed (Fig. 2, left) is +5.2 % (mean deviation +0.6 %), the power consumption of the chiller compressor (Fig. 2, middle) is calculated with a deviation of max. +7.4 % (mean +0.9 %) and the COP of the chiller (Fig. 2, right) with a deviation of max. -7 % (mean -0.7 %). Regarding the heat pump, the maximum deviations are -4.4 %, +1.9 %, +4.8 % and -2.4 % for the heating capacity, power consumption of the heat pump, COP of the heat pump and COP of the system, respectively, with mean deviations of -1.4 %, +0.5 %, -1.8 % and -0.4 % (Verdnik et al., 2022).

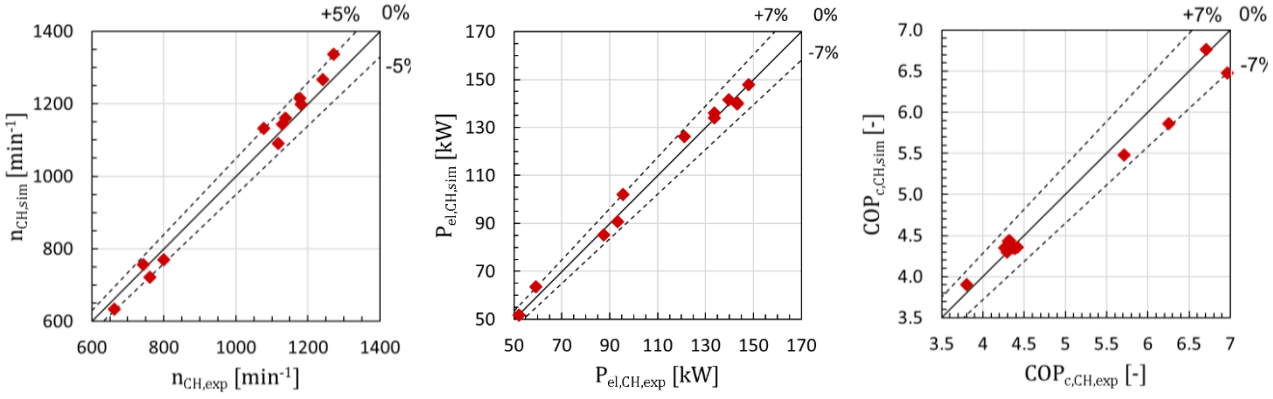

Figure 2: Comparison of measured (index "exp") and simulated (index "sim") chiller compressor speed (left), power consumption of the chiller compressor (middle) and COP of the chiller (right)

The transient validation of the chiller and heat pump in Verdnik et al. (2022) showed a deviation of +3 % for the energy consumption of the low pressure compressor, +3 % for the energy consumption of the high pressure compressor and -4 % for the thermal energy delivered by the heat pump during approximately 12.5 hours of operation. The transient validation of the whole system including the TES, where the heat pump is

operated according to the temperatures of the TES was re-checked due to minor changes in the heat pump startup procedure in the simulation model. The deviation of the simulation model to experimental data is +0.8 % for the energy consumption of the low pressure compressor, +0.1 % for the energy consumption of the high pressure compressor and -6 % for the thermal energy delivered by the heat pump during operation of approx. 12.5 hours. These deviations are smaller than the expected uncertainty of measurement (see Wagner et al. (2021) for details). The results of the validation show that the simulation model can be used to further investigate the steady and transient behaviour of the system.

4.2. Influence of the refrigerant subcooling

One peculiarity of the given hydraulic layout of the heat pump is that the flow through the subcooler is mixed with the rest of the heat sink after the condenser outlet (see Fig. 1 and Fig. 3, right). The simulated COP and condensing pressure of the heat pump when varying the refrigerant subcooling is shown in Fig. 3 (left) and the Q/t-Diagram of the subcooler, condenser and desuperheater in Fig. 3 (right). With the given hydraulic layout, an optimum subcooling exists. With the aid of the Q/t-Diagram it can be seen, that the increased flow through the subcooler to reach the desired subcooling reduces the flow through the condenser which in turn leads to the pinch point occurring at the refrigerant inlet of the condenser (state point HP4). If the refrigerant subcooling exceeds 22 K, this leads to an increase of the condensing pressure, demanding a higher compressor power consumption which causes the observed decrease of the COP.

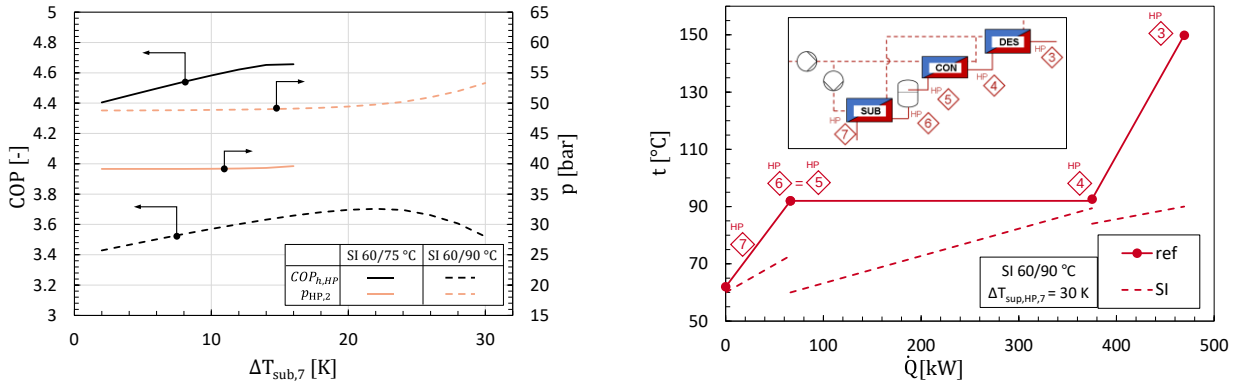

Figure 3: Influence of the refrigerant subcooling on the condensing pressure and COP (left) and Q/t-diagram (right) when mixing the heat sink after the condenser

In contrast, mixing the water outlet of the subcooler before the inlet of the condenser does not reduce the heat sink flow rate through the condenser and no increase in the condensing pressure of the heat pump occurs as shown in Fig. 4. In the Q/t-Diagram in Fig. 4 (right), a flatter slope of the heat sink in the condenser compared to Fig. 3 (right) can be observed.

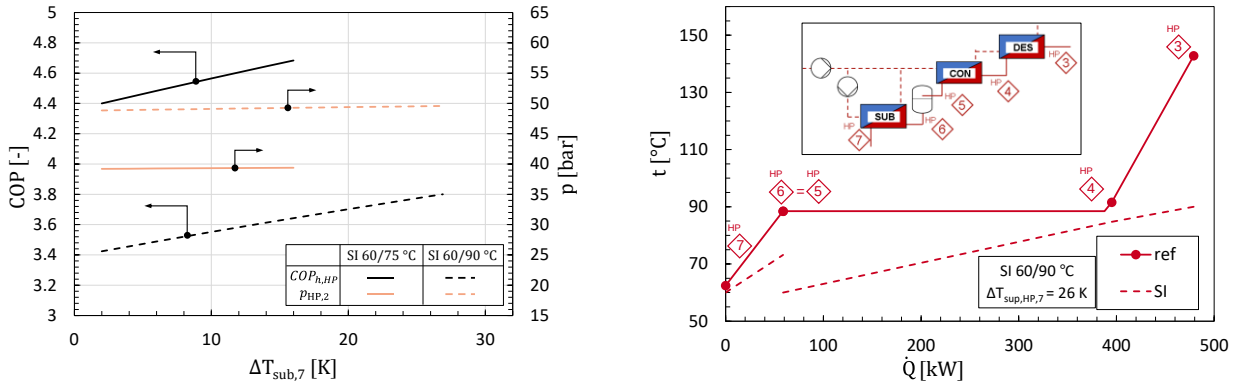

Figure 4: Influence of the refrigerant subcooling on the condensing pressure and COP (left) and Q/t-diagram (right) when mixing the heat sink before the condenser

4.3. Influence of the medium pressure

The following two simplified ways to vary the medium pressure i.e. discharge pressure of the low pressure compressor ($p_{CH,2}$) and suction pressure of the high pressure compressor ($p_{HP,1}$) are considered:

a) The pressure in the cooling tower and medium pressure receiver ($p_{CH,4} = p_{CH,9} = p_{CH,9}$) is kept constant and the medium pressure ($p_{CH,2}$) is varied by closing of the Valve$_{CH,4}$. In Fig. 5 (left), this is marked with solid lines ($p_{CH,4} \approx 8\ bar$).

b) The Valve$_{CH,4}$ is kept open and the medium pressure level ($p_{CH,2}$) is varied by adjusting the heat rejection. Fig. 5 (left) represents this option with dashed lines ($p_{CH,4} = var.$).

Regarding the operation of the chiller, it can be seen from Fig. 5 (left), that at the same medium pressure level option a) (closing Valve$_{CH,4}$) provides a higher cooling capacity than option b) (increasing the pressure in the cooling tower). Since the power consumption of the compressor remains constant, a higher COP of the chiller can be achieved. The increased cooling capacity can be explained by the lower enthalpy at the outlet of the medium pressure receiver at lower pressure levels, leading to a larger enthalpy difference available for evaporation after the isenthalpic throttling. Another important effect of the increased medium pressure is that the cooling capacity of the chiller decreases in both cases, with a stronger decrease for option b), demanding an increase of the chiller compressor speed to serve the same cooling load.

Regarding the heat pump, Fig. 5 (right) investigates the influence of the medium pressure on the heating capacity and COP of the heat pump for the heat sink temperature levels (inlet / outlet) of 60/75 °C, 75/90 °C and 60/90°C. As can be seen from Fig. 5 (right), both the heating capacity and the COP of the heat pump rise with increasing medium pressure.

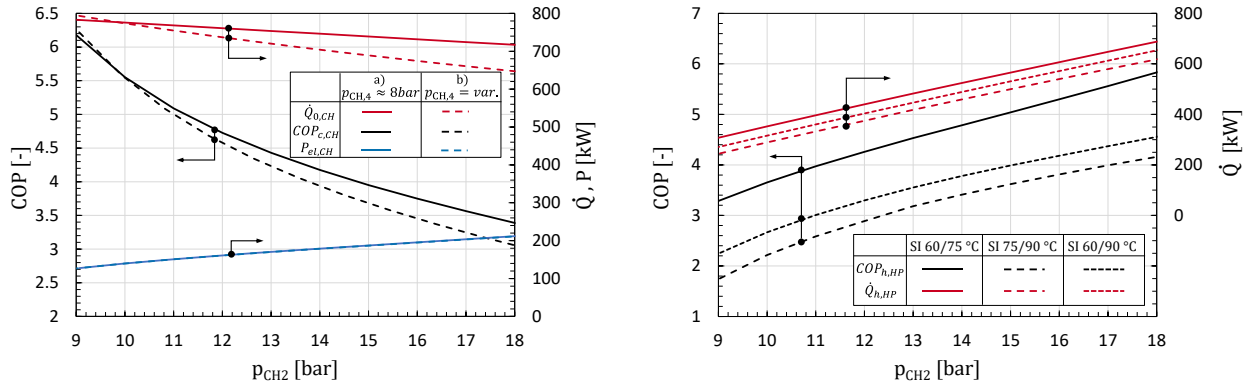

Figure 5: Influence of the medium pressure on the chiller operation (left) and heat pump operation (right)

Fig. 6 depicts the influence on the COP of the system at different cooling loads ($\dot{Q}_{0,CH}$ = 450 kW and 600 kW) for constant heat sink temperatures in Fig. 6 (left) and constant heat sink flow rate in Fig. 6 (right).

For constant heat sink temperatures and a cooling capacity of 450 kW an increase of the medium pressure leads to a higher COP of the system (solid lines in Fig. 6, left), while at a cooling capacity of 600 kW, the COP of the system remains almost constant (dashed lines). Fig. 6 (right) shows the influence of the medium pressure when the heat sink inlet temperature and the heat sink volume flow are constant. The increased heating capacity at higher medium-pressure levels lead to higher heat sink outlet temperatures, until the maximum high-pressure level of the heat pump is reached and the heating capacity is limited through the compressor speed. The increased heat sink outlet temperature reduces the COP of the heat pump, leading to the decrease of the system COP in Fig. 6 (right).

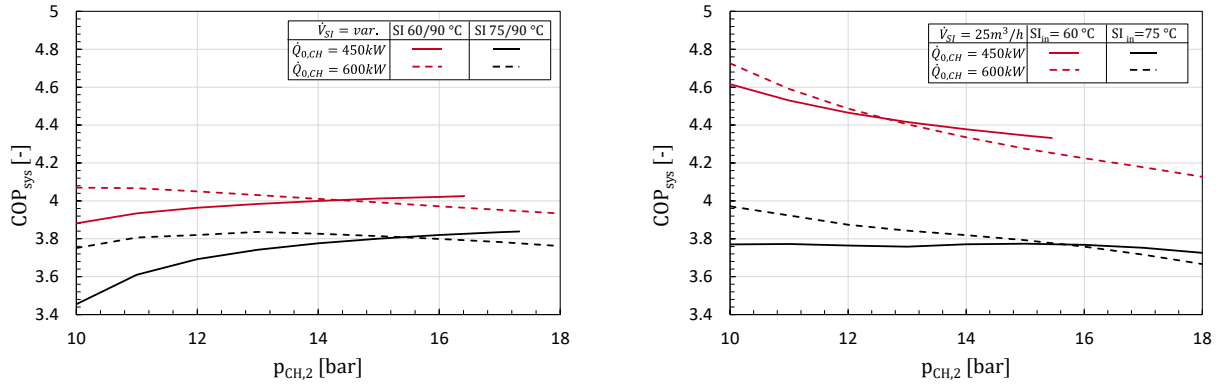

Figure 6: Influence of the medium pressure level on the COP of the system at constant heat sink temperatures (left) and constant heat sink volume flow (right)

As can be seen from Fig. 6, for the COP of the system, the relation of the cooling capacity to the heating capacity is relevant and determine how the influence of the medium pressure on the COP of the chiller (Fig. 5, left) and on the COP of the heat pump (Fig. 5, right) combine to the system COP.

4.4. Operating strategies of the heat pump

In the previous section, it was shown that an increase of the medium pressure increases the heating capacity and COP of the heat pump, while it decreases the cooling capacity and COP of the chiller. The influence on the system COP depends on the ratio of the capacities, where lower cooling capacities are beneficial for higher medium pressure levels. In the following section, the ability to cover load peaks of the CIP system by increasing the medium pressure level is investigated by means of a system simulation.

While the chiller operates at a constant cooling capacity of 450 kW, the heat pump supplying the TES is started when the temperature sensor inside the TES at the third position from the bottom ($t_{CIP,Stor,3}$ in Fig. 1) falls below a threshold and continues until the second sensor from the bottom ($t_{CIP,Stor,2}$ in Fig. 1) exceeds a threshold. The CIP load profile extracted from the TES is depicted in Fig. 7 and consists of a 60 minute load of 300 kW, followed by a 7 min peak of 900 kW and then 150 kW until the profile is restarted when switching off the heat pump. The flow rate to the CIP system is controlled so that the return temperature is 70°C. In order to evaluate the performance factors, the time period from switching the heat pump off (TES fully charged) to the next switching off is evaluated. For that time period, Fig. 7 depicts the CIP load, the supply temperature to the CIP system and the speed of the heat pump compressor, left for the nominal medium pressure of 13.5 bar ($t_{sat} = 35.0$°C) and right for an increased medium pressure of 18 bar ($t_{sat} = 45.4$°C). In both cases, if only the chiller is operating, the medium pressure is set to 9.5 bar.

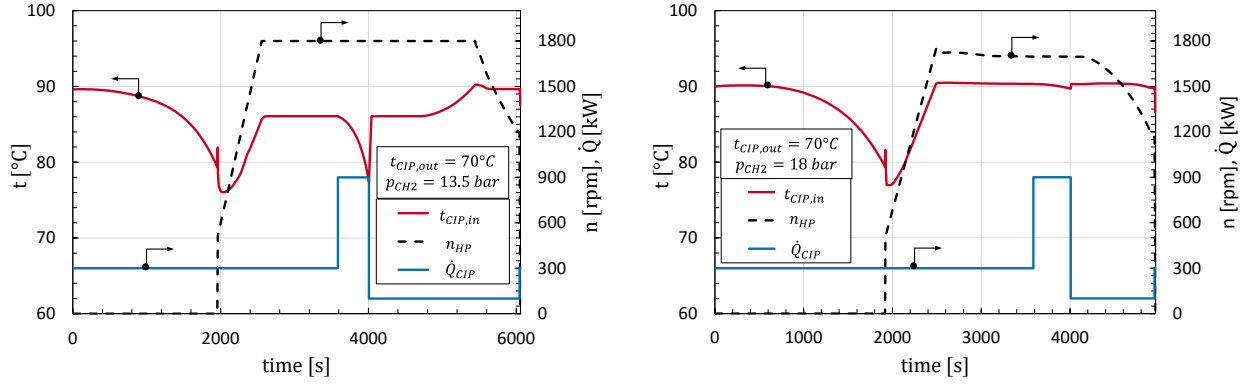

Figure 7: CIP load profile, CIP system supply temperate and heat pump compressor speed for 13.5 bar (left) and 18 bar medium pressure (right)

As can be seen from Fig. 7, the supply temperature to the CIP system drops before the heat pump starts in both cases. This drop could be avoided with an increased threshold to start the heat pump or with an advance

request in case a large CIP demand is expected. With 13.5 bar medium pressure, the temperature does not reach 90 °C again until approximately 5500 seconds after the start of the CIP load profile (see Fig. 7, left) and the CIP load peak causes a further drop of the temperature below 80°C. Increasing the medium pressure level to 18 bar allows to reach 90 °C supply temperature already after 2500 seconds and to hold it even during the load peak with only a marginal drop.

The influence on the system efficiency is investigated using performance factors that are based on the COP definitions in Eq. (8) to (10), integrating the relevant capacity or power to obtain the thermal or electric energy. As can be seen from Fig. 8, the increase of the medium pressure decreases the performance factor of the chiller from 5.1 to 4.1, increases the performance factor of the heat pump from 3.5 to 4.3 and in total decreases the performance factor of the system from 4.4 to 4.2. Besides this evaluated reduction in the system efficiency it should be noted that the increased supply temperature to the CIP system enabled by the increase in medium pressure can allow a further reduction of the steam consumption needed to heat the CIP system if the temperature supplied by the heat pump is not sufficient.

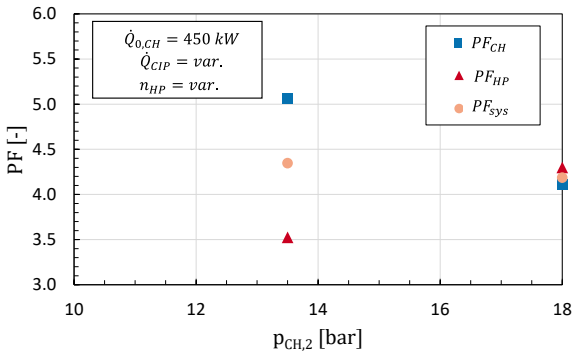

Figure 8: Performance factors of the chiller, heat pump and system at different medium pressure levels

CONCLUSIONS AND OUTLOOK

The introduced simulation model of a heat pump integrated into the refrigerant cycle of a chiller predicts the steady-state operation as well as the transient operation including a TES with sufficient accuracy to investigate the system behaviour. This is particularly useful to investigate the interrelationships between the chiller, the heat pump and the TES under varying CIP load profiles. By means of the simulation model, it was shown that the current hydraulic layout of the heat sink yields an optimum value for the refrigerant subcooling (with a decrease of the COP if the optimum is exceeded) and that this could be avoided with a different piping of the condenser and desuperheater. Further it was investigated how the heat sink temperatures and the medium pressure influence the COP of the chiller, the heat pump and the system, where the system efficiency also depends on the ratio between cooling and heating capacity.

Transient simulations prescribing the CIP load extracted from the TES showed, that by increasing the medium pressure level, the maximum supply temperature to the CIP system can be reached faster and held even under peak loads. Although this slightly decreases the evaluated system efficiency, it can be a valuable option if the steam demand of the CIP-system can be further reduced by reaching higher supply temperatures or if surplus electricity yield (e.g. from solar energy) is available.

Further activities covering the simulation model will be to optimize the heat pump operation with respect to scheduled production plans and derived CIP load profiles.

ACKNOWLEDGEMENTS

This study is part of the ENOUGH project, which has received funding from the European Union's Horizon 2020 research and innovation programme under grant agreement No 101036588.

NOMENCLATURE

1^{CH}…13^{CH}	State points of the chiller	out	Outlet
1^{HP}…13^{HP}	State points of the heat pump	p	Pressure (bar)
CH	Chiller	PF	Perfomance factor
CIP	Cleaning-in-Place	P	Electric power consumption of the compressor (kW)
COMP	Compressor	$\dot{Q}$	Thermal capacity (kW)
CON	Condener	ρ	Density ($kg \cdot m^{-3}$)
COP	Coefficient of Performance	rec	Receiver
DES	Desuperheater	ref	Refrigerant
EXV	Electric expansion valve	sat	Saturated
FI	Frequency inverter	SI	Heat sink
h	Specific enthalpy ($kJ \cdot kg^{-1}$)	sim	Simulation
HP	High pressure	SO	Heat source
HTWP/HP	High temperature heat pump	Stor / TES	Thermal Energy Storage
in	Inlet	sub	Subcooling
LP	Low pressure	SUB	Subcooler
exp	Experimentally	sys	System
MP	Medium pressure	t	Temperature (°C)
n	Rotational speed (rpm)	$\dot{V}$	Volume flow rate ($m^3 \cdot s^{-1}$)
NH_3	Ammonia		

REFERENCES

Akers, W.W., Deans, H.A., Crosser, O.K., 1959. Condensing heat transfer within horizintal tubes. Chemical Engineering Progress, 89–90.

Bakalis, S., Malliaroudaki, M. I., Hospido, A., Guzman, P., 2019. Predictive modelling tools to evaluate the effects of climate change on food safety (PROTECT). State-of-the art in energy use and sustainability of the dairy industry. Deliverable number: D5.1. URL: https://ec.europa.eu/research/participants/documents/downloadPublic?documentIds=080166e5cab758ff&appId=PPGMS (1.9.2022)

Eurostat, 2018. Agriculture, forestry and fishery statistics: 2018 edition, European Union, Luxembourg. https://ec.europa.eu/eurostat/documents/3217494/9455154/KS-FK-18-001-EN-N.pdf/a9ddd7db-c40c-48c9-8ed5-a8a90f4faa3f?t=1558692068000 (22.4.2021).

IEA, 2022. The Future of Heat Pumps, International Energy Agency, Paris, https://www.iea.org/reports/the-future-of-heat-pumps (4.2.2023).

Keller, R., Jungbluth, N., Eggenberger, S., 2016. Milk Processing – Life cycle assessment of a detailed dairy model and recommendations for the allocation to single products. Proc. 10th International Conference on Life Cycle Assessment of Food (LCA Food 2016), Dublin, Ireland.

Longo, G.A., Mancin, S., Righetti, G., Zilio, C., 2015. A new model for refrigerant boiling inside Brazed Plate Heat Exchangers (BPHEs). International Journal of Heat and Mass Transfer 91, 144–149. https://doi.org/10.1016/j.ijheatmasstransfer.2015.07.078.

Martin, H., 2010. Pressure Drop and Heat Transfer in Plate Heat Exchangers, in: Verein Deutscher Ingenieure (Ed.), VDI Heat Atlas. Springer.

TLK-Thermo, 2022a. TIL Suite V 3.13.0. TLK-Thermo GmbH, Braunschweig, Germany, Braunschweig, Braunschweig.

TLK-Thermo, 2022b. TIL Suite Heat Storage AddOn V 3.13.0. TLK-Thermo GmbH, Braunschweig, Germany, Braunschweig, Braunschweig.

Verdnik, M., Wagner, P., Wernhart, M., Rieberer, R., 2022. Modellbasierte Analyse einer NH3-HTWP in einem Molkereibetrieb. Proc. Deutsche Kälte-Klima-Tagung 2022, Magdeburg. https://doi.org/10.5281/zenodo.7543933

Wagner, P., Verdnik, M., Rieberer, R., Demmerer, T., Blaser, M., 2021. Add-on NH3-Hochtemperatur-Wärmepumpe zur Abwärmenutzung einer bestehenden Kälteanlage. Proc. Deutsche Kälte-Klima-Tagung 2021, Dresden.

Data Availability Statement: Data available in a publicly accessible repository (https://doi.org/10.5281/zenodo.7627820)